

ADVANCED ROBOTICS

Design Methodology of Hydraulically-driven Soft Robotic Gripper for a Large and Heavy ObjectKo Yamamoto^a ^{*1}, Kyosuke Ishibashi^a, Hiroki Ishikawa^a and Osamu Azami^a^aDepartment of Mechano-informatics, The University of Tokyo 7-3-1 Hongo, Bunkyo-ku, Tokyo 113-8656, Japan**ABSTRACT**

This paper presents a design methodology of a hydraulically-driven soft robotic gripper for grasping a large and heavy object — approximately 10 - 20 kg with 20 - 30 cm diameter. Most existing soft grippers are pneumatically actuated with several hundred kPa pressure, and cannot generate output force sufficient for such a large and heavy object. Instead of pneumatic actuation, hydraulic actuation has a potential to generate much larger power by several MPa pressure. In this study, we develop a hydraulically-driven soft gripper, in which its basic design parameters are determined based on a mathematical model that represents the relationship among the driving pressure, bending angle, object mass and grasping force. Moreover, we selected materials suitable for grasping a heavier object, based on the finite element analysis result of the detailed design. We report experimental results on a 20 kg object grasping and closed-loop control of the finger bending angle.

KEYWORDS

Soft Robotic Gripper; Hydraulics; Modeling and Control for Soft Robots

1. Introduction

Soft robotic grippers have gained significant attention due to their adaptability to various objects [1,2] and have a lot of applications including food industry, agriculture, healthcare, manufacturing, logistics [3–5]. Especially, soft grippers are suitable for a lightweight, delicate and fragile object with irregular shape, which traditional rigid robotic grippers cannot grasp safely and effectively. Several types of soft grippers have been developed, each utilizing different materials, actuation methods, and design principles, such as pneumatically actuated grippers [6], electroactive polymer grippers [7,8], shape memory alloy (SMA) grippers [9], magnetorheological (MR) fluid grippers [10], electroadhesion grippers [11], gripper with Gecko-inspired adhesives [12], soft grippers with jamming mechanisms [13] and Origami-inspired grippers [14].

However, most existing soft grippers are pneumatically actuated with several hundred kPa pressure, and cannot generate output force sufficient for such a large and heavy object that usually human is capable of — approximately 10 - 20 kg with 20 - 30 cm diameter. According to the Health and Safety Executive in the UK [15], a

^{*1}CONTACT Ko Yamamoto. Email: yamamoto.ko@ynl.t.u-tokyo.ac.jp

© 2026 Copyright held by the owner/author(s). This is an original manuscript of an article published by Taylor & Francis in Advanced Robotics on 8th Jan. 2026, available at: <https://doi.org/10.1080/01691864.2025.2608943>

human worker is encouraged to carry an object less than 16 kg for woman and 25 kg for man to reduce the risk of injury. There are a few attempts to develop a soft gripper that can grasp a heavy object. Yap et al. [16] developed a soft robot gripper capable of grasping objects up to 10 cm and 5 kg. However, it was reported [16] that its output power decreases as the target object size increases. Hwang et al. [17] developed a gripper using electro-adhesion that was capable of 16.8 kg. However, this gripper was not suitable for an object with rough and moist surfaces.

Instead of pneumatic actuation, hydraulic actuation has a potential to generate much larger power by several MPa pressure. Previously, Hagiwara et al. [18] developed a hydraulically-driven soft gripper capable of grasping a 5 kg object. Then, we developed a prototype of a hydraulically-driven soft gripper for transporting large and heavy vegetables in a vegetable factory [19,20]. However, those studies focused on the design of the soft finger with durability of high pressure, and the analysis on the actuation performance by a hydraulic pump. In the design and control of a soft gripper, it is important to analyze the total system mechanics consisting of hydraulic pump, soft fingers and target object. In [21], we constructed a mathematical model of the soft gripper including the actuation unit, and showed that the oil reservoir with rubber sheet can boost the pump actuation and decrease the pressure necessary for bending the soft fingers.

In this paper, we present a design methodology of a hydraulically-driven soft robotic gripper for grasping an object with 10 to 20 kg weight and 20 to 30 cm diameter. We estimate the maximum payload based on the previously developed model and the friction condition. Then, we conduct a strength analysis by finite element method (FEM) in the detailed design of the soft gripper and select appropriate material for grasping a 20 kg object. Finally, we report experimental results on the 20 kg payload test, grasping various objects, and a closed-loop control based on the proposed model.

The rest of this paper is organized as follows. Section 2 presents the basic structure of the soft gripper and its mathematical model. Section 3 details the design based on the parameters obtained in Section 2 and provides the FEM analysis. Section 4 reports the experimental validations. Finally, Section 5 provides discussions on the obtained results, and Section 6 concludes this paper.

Portions of this paper were previously presented in [21], including the basic of mathematical model (Section 2.2), and the structure of the soft gripper (Section 3.1). Whereas the previous paper [21] focused on the feedback control of the bending angle and the evaluation of the grasping flexibility achieved by the feedback, the main contribution of this study is to present a design methodology to achieve high payload such as 20 kg and to provide its experimental validations.

2. Design Methodology of Hydraulically-driven Soft Robot Gripper

2.1. Structure of Hydraulically-driven Soft Robot Gripper

Fig. 1 shows the structure of the hydraulically-driven soft robot gripper including its actuation system. A hydraulic pump generates a differential pressure, in which the high- and low-pressure sides are connected to soft fingers and oil reservoir, respectively. The differential pressure sends the oil from the reservoir to the soft fingers and pressurizes the inner flow path of the soft finger. We employ the fiber-constrained design [22,23], in which the radial expansion is constrained by wrapping a thread around the finger, as shown in Fig. 1 (b). When the inner flow path is pressurized, the fin-

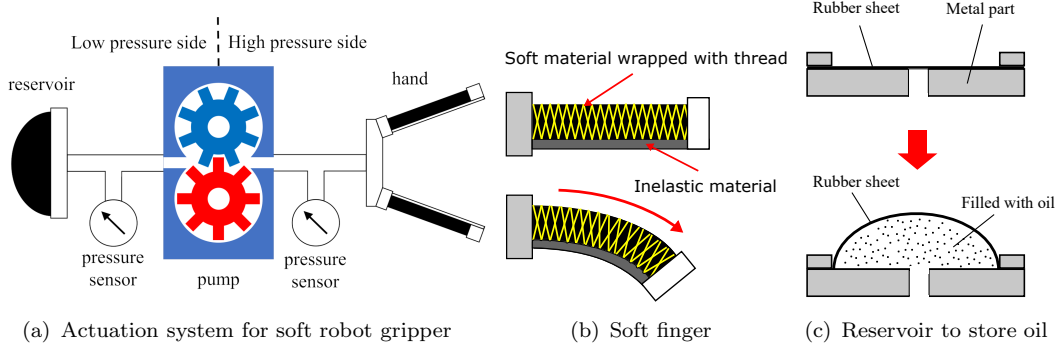


Figure 1. (a) Soft fingers are connected to the high-pressure side of the hydraulic pump while a reservoir is connected to the low-pressure side. The pump generates differential pressure, sending oil from the reservoir to the soft fingers. (b) Structure and bending mechanism of fiber-constrained soft finger. Fiber-constrained soft fingers utilize the expansion of soft materials under pressure and deform only in a certain direction by embedding inelastic materials. (c) Structure of reservoir. The reservoir consists of a circular sheet made of NBR, along with a ring-shaped metal part and base.

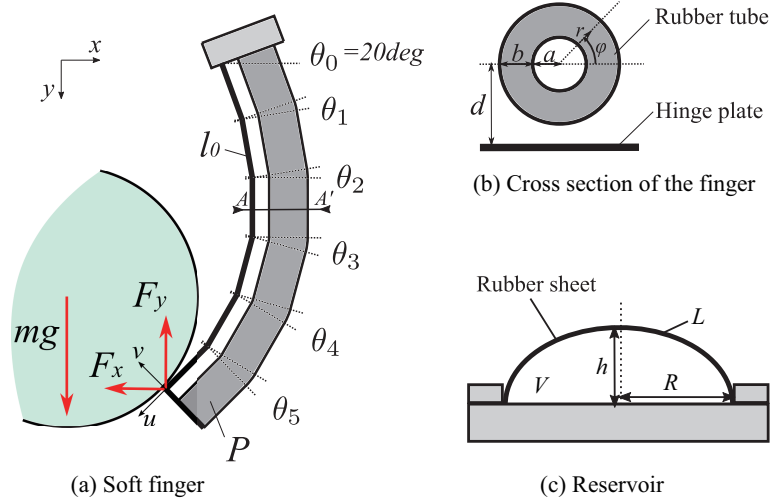


Figure 2. Geometric Model of hydraulic soft gripper. (a) Soft finger. (b) Cross section of finger. (c) Reservoir made of rubber sheet. Reservoir consists of a circular sheet made of NBR, along with a ring-shaped metal part and base, as shown in Fig. 1 (b).

ger expands only in the axial direction. This expansion is transformed into a bending deformation because one side of the finger is constrained by an inelastic part. Fig. 1 (c) illustrates the structure of the oil reservoir, consisting of a circular sheet made of NBR and a ring-shaped metal part and base.

2.2. Modeling of Hydraulically-driven Soft Robot Gripper [21]

We formulated a mathematical model to represent the relationship among the driving pressure, bending angle of a finger, and grasping force on a target object. Renda et al. [24,25] proposed a PCS model that divides a flexible rod structure into a finite number of segments with constant strain, deriving its kinematics and dynamics. Polygerinos et al. [26,27] modeled fiber-reinforced soft fingers assuming constant curvature, while Mustaza et al. [28] developed a manipulator with fiber-constrained actuators and used

Table 1. Parameters and Symbols of the gripper model.

Param	Description	Value
θ_0	Inclination of the base link of the finger	20deg
l_0	Initial length of the finger	180mm
a	Internal diameter of the rubber tube	4mm
b	Thickness of the rubber tube	5mm
d	Distance between hinge plate and rubber tube	15mm
R	Radius of reservoir sheet	24mm
t	Thickness of reservoir sheet	1mm
V_0	Initial volume of oil stored in reservoir	17.8cm ³
n	The number of finger attached to the gripper	4
n_s	The number of hinge joint in a finger	5
μ_{sf}	Initial shear modulus of rubber tube (finger)	1.15MPa
μ_{sr}	Initial shear modulus of rubber sheet (reservoir)	1.15MPa
μ_f	Coefficient of static friction	0.7

Symbol	Description
P	Pressure of the inner side of the finger
F_x, F_y	Force applied to the tip of the finger
$(\theta_1, \dots, \theta_{n_s})^T$	Bend angles between the hinge plate
$\theta = \sum \theta_i$	Bend angle of finger
m	Mass of the grasping object

Lagrange's equations for dynamic modeling. Sedal et al. [29] derived equations for fiber-constrained soft actuators, relating various mechanical parameters under static conditions using continuum mechanics. However, these studies focused on modeling the soft finger alone, without considering the entire gripper system. In [21], we proposed a mathematical model that includes both the soft fingers and the reservoir and demonstrate that the reservoir's elasticity contributes to efficient actuation.

Fig. 2 shows a geometric model of a soft finger, and Table 1 lists variables used in the proposed model. We simplified the finger structure based on the following assumptions:

- The soft robot gripper has multiple fingers, but we assume that all fingers have the same deformation for simplicity.
- The inelastic part is divided into multiple segments connected by revolute joints.
- When the gripper grasps an object, the weight is supported only at the fingertips.
- The contact forces are equally distributed among the fingertips.

From the virtual work principle, the virtual work by the pressure P and contact force (F_x, F_y) is equal to the variations of the strain energies in the fingers and the reservoir. This relationship is represented as

$$P\Delta Q + n(F_x\Delta x + F_y\Delta y) = n\Delta W_f + \Delta W_r. \quad (1)$$

Outline of each term is summarized as follows:

- The first term on the left-hand side represents the virtual work produced by the hydraulic pump, where ΔQ denotes the flow rate in the finger.
- The second and third terms account for the work produced by the contact force,

where n is the number of fingers, and Δx and Δy are the virtual displacements of the fingertip position.

- In the first term on the right-hand side, ΔW_f is the variation in strain energy of the finger rubber tube.
- ΔW_r is the variation in strain energy in the reservoir sheet.

The details are summarized in the following subsections.

2.2.1. Virtual Work by Hydraulic Pump

The virtual work by the hydraulic pump is given by $P\Delta Q$, where Q is the internal volume of the fingers. Let θ_i ($i = 0, \dots, n_s$) denote the bending angle of the i -th segment. Assuming a finger has a simple cylindrical shape as shown in Fig. 2, Q is calculated as

$$Q = na^2\pi(l_0 + d\theta) \quad (2)$$

where

$$\theta := \sum_i \theta_i. \quad (3)$$

Therefore, the virtual work $P\Delta Q$ is calculated as

$$P\Delta Q = Pna^2\pi d\Delta\theta \quad (4)$$

where $\Delta\theta$ is the variation of θ .

2.2.2. Variation in Strain Energy of a Finger

Next, we consider the variation in strain energy ΔW_f of the NBR tube. The strain energy W_f of a finger is calculated based on the Neo-Hookean model [30] as

$$W_f = \int \frac{\mu_{sf}}{2} (I_1 - 3) dV \quad (5)$$

where I_1 is the first invariant of deviation strain, represented using the axial, radial and circumferential deformation rates $\lambda_1, \lambda_2, \lambda_3$ as

$$I_1 = \lambda_1^2 + \lambda_2^2 + \lambda_3^2. \quad (6)$$

In this study, $\lambda_2 = 1$ is satisfied because the radial direction is constrained. Moreover, $\lambda_1\lambda_2\lambda_3 = 1$ is satisfied because NBR is an incompressible material. Therefore, the values of λ_1, λ_2 and λ_3 are summarized as

$$\lambda_f := \lambda_1, \lambda_2 = 1, \lambda_3 = \frac{1}{\lambda_f} \quad (7)$$

where λ_f is an alias of λ_1 , Considering a polar coordinate r and ϕ in the cross section A-A' shown in Fig. 2, λ_f is calculated as

$$\lambda_f = \frac{l_0 + \{d + (a + r) \sin \phi\}\theta}{l_0} \quad (8)$$

From (5)-(8), we can represent ΔW_f as

$$\Delta W_f = \mu_{sf} \zeta_f(\theta) \Delta \theta \quad (9)$$

where

$$\zeta_f(\theta) := \int_0^{2\pi} \int_0^b (\lambda_f - \frac{1}{\lambda_f^3}) \frac{d\lambda_f}{d\theta} \cdot l_0(a + r) dr d\phi. \quad (10)$$

2.2.3. Variation in Strain Energy of Reservoir Sheet

The strain energy in the reservoir sheet W_r can be expressed as

$$W_r = \int \frac{\mu_{sr}}{2} (I_1 - 3) dV \quad (11)$$

in a manner similar to (5). Because the rubber sheet undergoes biaxial tensile deformation, the values of λ_1, λ_2 and λ_3 are given as

$$\lambda_r := \lambda_1 = \lambda_2, \lambda_3 = \frac{1}{\lambda_r^2} \quad (12)$$

where λ_r is an alias of λ_1 or λ_2 .

Fig. 2 (c) shows a schematic diagram of the reservoir. Assuming that the rubber sheet deforms into an ellipse, the circumference $L(h)$ of the ellipse can be formulated using Ramanujan's approximation [31] as

$$2L(h) = \pi \{3(R + h) - \sqrt{(R + 3h)(h + 3R)}\} \quad (13)$$

where R and h are the radius and height of the reservoir, respectively, calculated as

$$h = \frac{3}{2\pi R^2} V, \quad (14)$$

$$V = V_0 - a^2 \pi d n \theta \quad (15)$$

Then, λ_r can be written as

$$\lambda_r = \frac{L(h)}{2R} \quad (16)$$

From (11)-(15), we can calculate ΔW_r as

$$\Delta W_r = \mu_s \zeta_r(\theta) \Delta \theta \quad (17)$$

where

$$\zeta_r(\theta) := 2(\lambda_r - \frac{1}{\lambda_r^5}) \frac{d\lambda_r}{d\theta} \cdot \pi R^2 t. \quad (18)$$

2.2.4. Virtual Work by Grasping Force

Let $\Delta\boldsymbol{\theta}$ denote a vector storing the virtual displacements of joint angles, defined as

$$\Delta\boldsymbol{\theta} = [\Delta\theta_1 \ \cdots \ \Delta\theta_{n_s}]^T. \quad (19)$$

Then, the relationship between the virtual displacement of the finger tip and $\Delta\boldsymbol{\theta}$ is obtained as

$$\begin{bmatrix} \Delta x \\ \Delta y \end{bmatrix} = \begin{bmatrix} \mathbf{J}_x \\ \mathbf{J}_y \end{bmatrix} \Delta\boldsymbol{\theta} \quad (20)$$

where \mathbf{J}_x and \mathbf{J}_y are the Jacobian matrices.

In general, $\Delta\boldsymbol{\theta}$ is not uniquely determined when given a displacement of the total bending angle $\Delta\theta$. Hence, we represent $\Delta\boldsymbol{\theta}$ using a coefficient vector \mathbf{w} as

$$\Delta\boldsymbol{\theta} = \mathbf{w}\Delta\theta \quad (21)$$

$$\mathbf{w} := [w_1 \ \cdots \ w_{n_s}]^T. \quad (22)$$

Note that w_1, \dots, w_{n_s} satisfy the following equation.

$$\sum_{i=1}^{n_s} w_i = 1 \quad (23)$$

The simplest way to determine these coefficients is to set all coefficients to the same value: $w_i = \frac{1}{n_s}$. In reality, however, this does not always apply. In particular, these coefficients are different when the fingers grasping an object. In [21], we set the value of \mathbf{w} based on an FEM result of the detailed design for a more detailed analysis, which is also mentioned in Section 3.2.

2.2.5. Total Virtual Work Relationship and Grasping Condition

As we assumed in the beginning of this section, the contact forces are equally distributed among the fingertips. Therefore, F_y is given by

$$F_y = \frac{mg}{n}. \quad (24)$$

Substituting (4), (9), (17), (20) and (21) into (1) and eliminating $\Delta\theta$ yield the following relation among P, θ, F_x and m .

$$P(\theta, m, F_x) = \frac{1}{na^2\pi d} \{n\mu_{sf}\zeta_f(\theta) + \mu_{sr}\zeta_r(\theta) - (nF_x\mathbf{J}_x + mg\mathbf{J}_y)\mathbf{w}\} \quad (25)$$

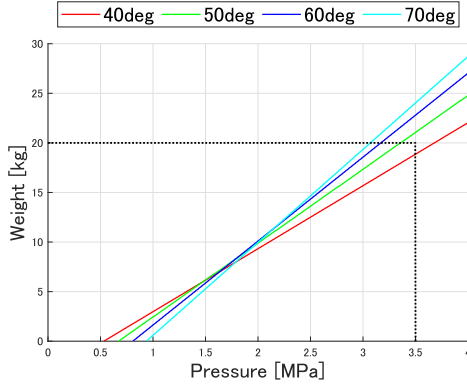


Figure 3. Maximum payload of soft gripper estimated for bending angles of 40° , 50° , 60° , and 70° .

When the gripper is not grasping an object, we can derive the following relationship between P and θ , substituting $F_x = F_y = 0$ into (25).

$$P = f(\theta) = \frac{1}{na^2\pi d}(n\mu_{sf}\zeta_f(\theta) + \mu_{sr}\zeta_r(\theta)) \quad (26)$$

2.3. Maximum Payload Estimation based on Detailed Parameter Values

In the presented model, we first determined the values of the parameters l_0 and θ_0 to grasp about 20 cm diameter object. Because it is hard to systematically optimize the other detailed parameters, we determined those values through cycles of prototyping and checking if the requirements were satisfied, including trial and error. Table 1 lists the determined parameters.

Using the determined parameters, we calculate the maximum payload. Grasping an object without slipping requires the following conditions on the friction force:

$$F_v = F_x \cos(\theta - \theta_0) + F_y \sin(\theta - \theta_0) \quad (27)$$

$$F_u = F_x \sin(\theta - \theta_0) - F_y \cos(\theta - \theta_0) \quad (28)$$

$$-\mu_f F_v \leq F_u \leq \mu_f F_v \quad (29)$$

where F_u and F_v are the contact forces w.r.t. the uv coordinates in Fig. 2, and μ_f is the maximum static friction force coefficient.

Fig. 3 (a) shows the maximum payload calculated for bending angles of 40° , 50° , 60° , and 70° . It is seen that the maximum payload can be more than 20 kg when the pressure is 3.5 MPa.

3. Development of Hydraulic Soft Gripper

3.1. Detailed Structure of Hydraulically-driven Soft Gripper [21]

Fig. 4 shows the developed soft gripper. The width and height are 278 mm and 346 mm, respectively, with a total weight of approximately 2.8 kg, including the actuation unit (1.67 kg) consisting of a hydraulic pump and electric motor. We used a hydraulic

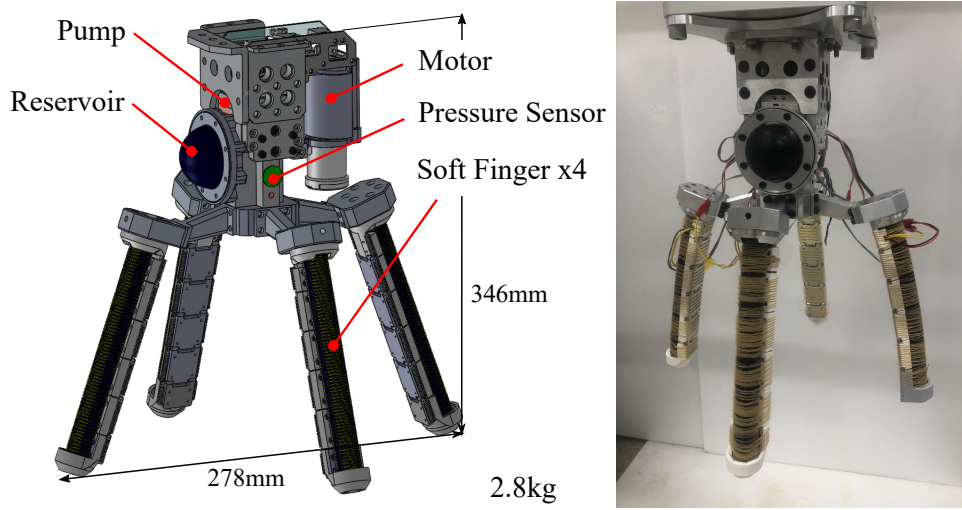


Figure 4. Four-finger hydraulic soft robot gripper. The gripper is composed of soft fingers, pressure sensors, a reservoir for storing oil, a hydraulic pump, and a motor for driving the pump.

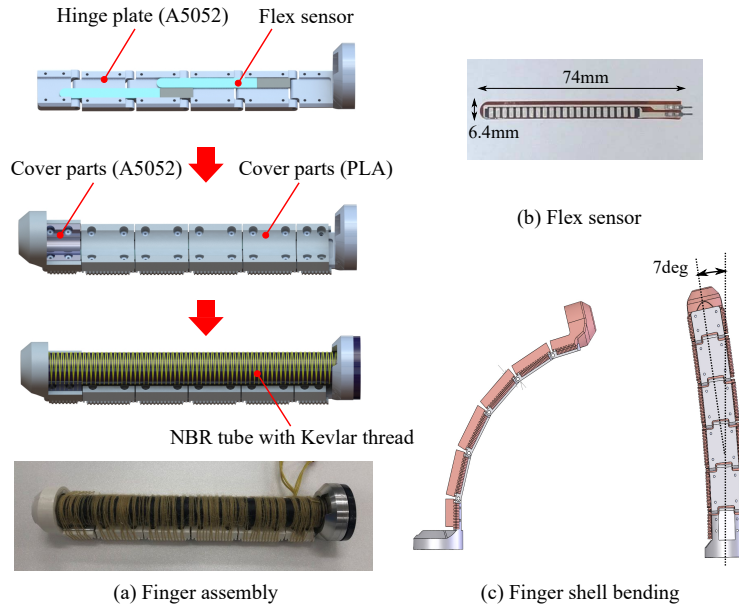


Figure 5. Fabricated soft finger. (a) Structure of soft finger, (b) Resistive flexible sensor, (c) Image of finger shell bending.

pump (dimensions: 42 x 47.2 x 22.8 mm; weight: 228 g) developed in [32]. Two pressure sensors are equipped on the high- and low-pressure sides of the pump flow path, which enables us to measure the differential pressure for the pressure control by the motor current.

Fig. 5 shows the structure of the developed soft finger. The fabrication process is summarized as follows:

- (1) The exoskeleton parts of the fingers are made of A5052 to prevent excessive twisting in the axial direction. These parts are connected by hinge joints. Two flexible sensors (SPECTRASYMBOL-006, Spectra Symbol, Inc) shown in Fig.

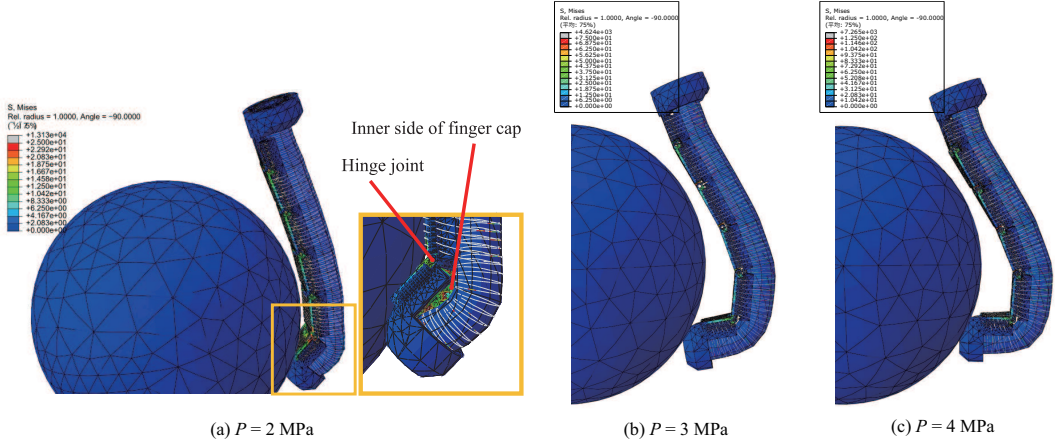


Figure 6. FEM simulations of an object grasping under pressure of 2.0 MPa, 3.0 MPa and 4.0 MPa. This figure indicates that stress is concentrated at the cap and hinge points at the tips of the fingers.

5 (b) are inside the exoskeleton to measure the bending angle.

- (2) Next, a 3D-printed cover is attached to each exoskeleton part. The covers are made of PLA, except for the fingertip, which is made of A5052 based on an FEM analysis discussed in the next subsection.
- (3) Finally, an NBR tube ($\phi 18 \times 180$ mm, and 4 mm thick) constrained by Kevlar thread is inserted into the exoskeleton parts.

3.2. FEM Analysis

Based on the detailed design of the developed gripper, we conducted an FEM analysis to select suitable materials for the necessary parts, and also determine the specific values of \mathbf{w} in the mathematical model. Using the parameters listed in Table 2, we simulated a finger movement setting the driving pressure to 2.0 MPa, 3.0 MPa and 4.0 MPa.

Fig. 6 shows the results of the FEM analysis, and Table 3 summarizes the maximum stress in the fingertip components. When applying 4.0 MPa pressure, the maximum stress was 235.4 MPa at the fingertip cap and 170.3 MPa at the hinge joint in the fingertip. Since the fracture strength of PLA is 55 MPa, we selected A5052 for these parts due to its higher strength. Moreover, the strength of NBR with 70 Shore A hardness is 12.7 MPa, which affords to the driving pressure.

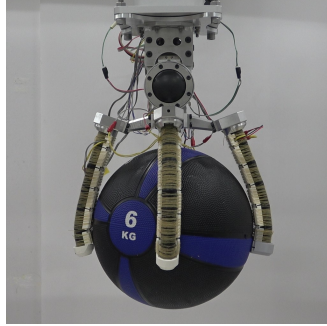
It is observed from Fig. 6 that the 5th joint bent more largely than the other joints when the pressure is increased. We consider that this is because the fingertip contacts with the object on a fixed point. This result implies that the assumption in the previous section does not apply — all joints do not have the same angle but different angles. Therefore, we determine the value of the coefficient vector \mathbf{w} based on the FEM result in [21]. In the FEM simulation, the values of $\Delta\theta_i$ ($i = 1, \dots, 5$) were calculated in each step of the simulation, and we used those values to determine \mathbf{w} . As a result, the value of \mathbf{w} was set as $\mathbf{w} = (-0.2, 0.0, 0.1, 0.3, 0.8)^T$. Moreover, the modeling using this value of \mathbf{w} was validated in [21] based on a preliminary experiment on a 6 kg object, which will be shown in Section 4.

Table 2. Parameter used in FEM simulation

Mooney-Rivlin coefficient of NBR tube	$C_{10} = 0.41, C_{01} = 0.43$
Young's modulus of A5052 metal parts	68 MPa
Poisson's ratio of A5052 metal parts	0.33
Young's modulus of PLA parts	3.5 MPa
Poisson's ratio of PLA parts	0.3
Young's modulus of Kevlar thread beam	31 MPa
Poisson's ratio of Kevlar thread beam	0.36
Radius of Kevlar thread beam	0.2 mm

Table 3. Comparison of maximum stress and material fracture strength applied to fingers.

Pressure applied to the finger	2.0MPa	3.0MPa	4.0MPa
Maximum stress of a cap part of the finger	124.8MPa	153.4MPa	235.4MPa
Maximum stress of a hinge structure	82.3MPa	114.4MPa	170.3MPa
Maximum stress of a rubber tube	3.3MPa	3.9MPa	4.9MPa
PLA strength		55MPa	
A5052 strength		260MPa	
NBR strength		12.7MPa	

**Figure 7.** Pre-experiment to re-estimate the maximum payload. In this experiment, we tested a grasping of a 6 kg dumbbell.

4. Experimental Validations

4.1. Maximum Payload

We experimentally validate the maximum payload of the developed gripper. Before the experiment, we re-estimate the maximum payload, which was originally presented in Fig. 3, based on the mathematical model using the value of w determined as mentioned in the previous section. The relationship between the finger angle and the grasping force using this value was validated also in [21] with a preliminary experiment using the 6 kg object (shown in Fig. 7). Fig. 8 shows the updated result of the maximum payload to a given finger bending angle. Given a pressure of 2.0 MPa, the maximum payload is estimated as 27 kg at 40° and 20 kg at 70°.

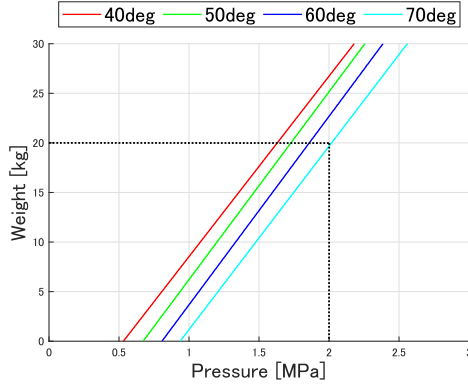


Figure 8. Maximum payload of four-finger soft gripper when wrapping an object. For a pressure of 2.0 MPa, the gripper can grasp a maximum weight of 27 kg at 40 degrees and a maximum weight of 20 kg at 70 degrees.

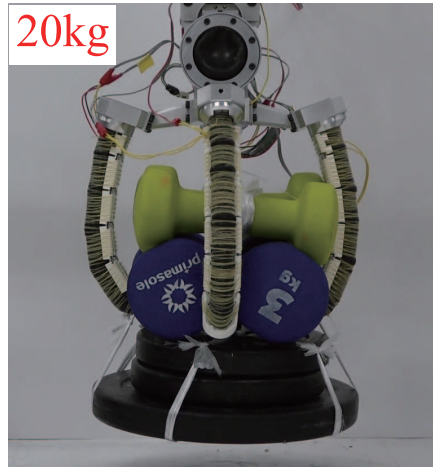


Figure 9. Experimental scene of 20 kg payload test. In this experiment, a four-finger soft gripper grasped a set of dumbbells whose total weight is 20 kg and held it for 10 s by the 2.0 MPa pressure control.

Fig. 9 shows an experimental scene in which the developed soft gripper grasps a set of dumbbells whose total weight is 20 kg and holds it for 10 s. The results of the 20 kg payload is consistent with the result of Fig. 8.

Although we set the value of w based on the FEM result with a 240 mm diameter object, this condition does not always apply to unknown shape object. Indeed, the shape of the 20 kg object was largely different from the 240 mm diameter sphere object. Rather, this result shows that the payload estimation based on the developed model can be applied to such a different condition as the softness of the developed hand absorbed an uncertainty.

4.2. Examples of Grasping Various Objects

Moreover, we validated the adaptability of the developed soft gripper to various objects as shown in Fig. 10, including some large size vegetables. The simple pressure control enabled the soft gripper to grasp various industrial products including Fig. 10(a)(c) cable reels and (b) a bucket. One of possible applications of this gripper is a picking task in a vegetable factory. We also demonstrated (d) Chinese cabbage, (e) cabbage

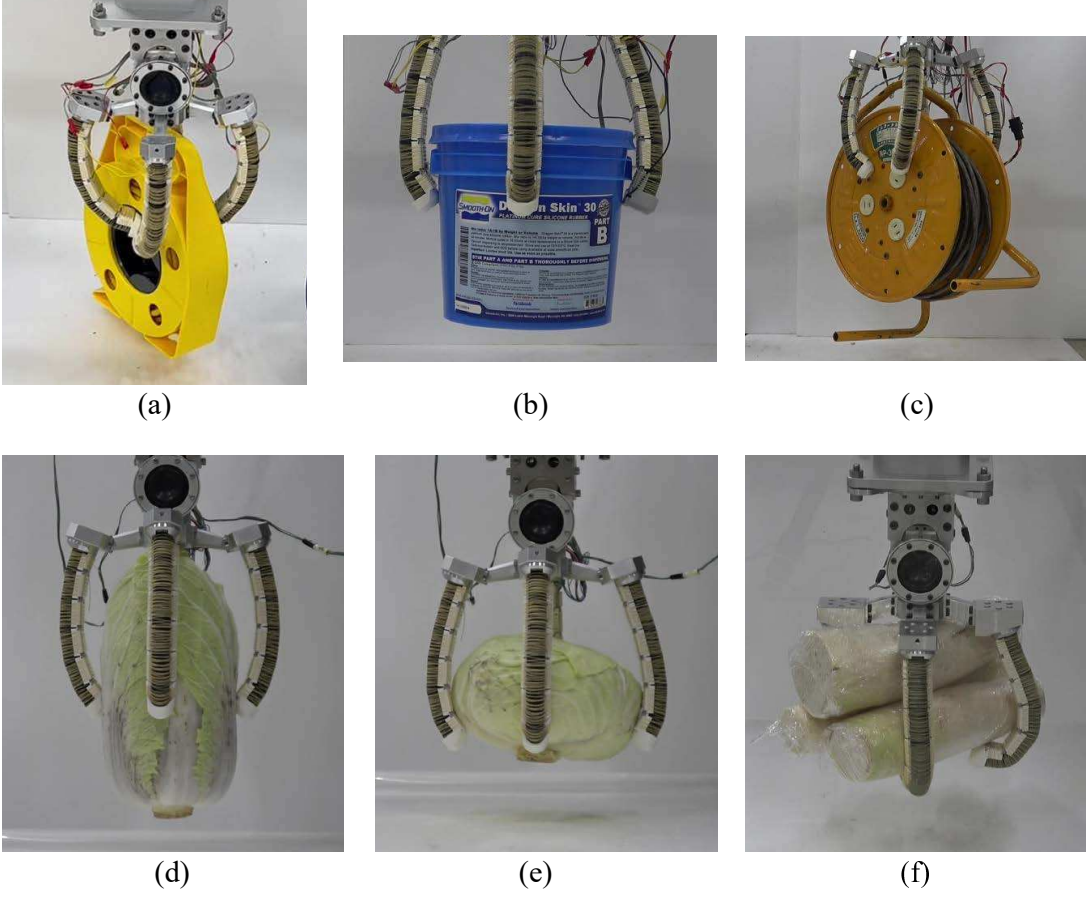


Figure 10. Grasping various objects: (a) cable reel (5.8 kg), (b) bucket (4 kg), (c) cable reel (6 kg), (d) Chinese cabbage (2.6 kg), (e) cabbage (2.3 kg), and (f) three radishes (\simeq 2.1 kg).

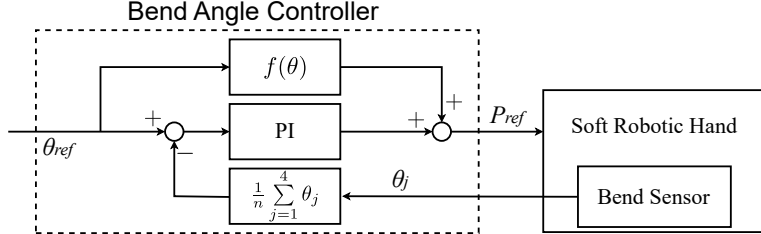


Figure 11. Two-degree-of-freedom control of the bending angle of the fingers using the relationship between θ and P obtained by (26). The average angle of fingers was controlled to follow the commanded angle since each finger is connected to the same flow path.

and (f) radishes were grasped by the developed gripper. These results show that the developed hand achieved not only high payload but also high adaptability to variety in different conditions of shape and surface.

4.3. Closed-loop Control of Finger Bending Angle

Finally, we validated a feedback control of the finger angles. While we demonstrated a robustness of the feedback control to horizontal-direction disturbance in [21], we

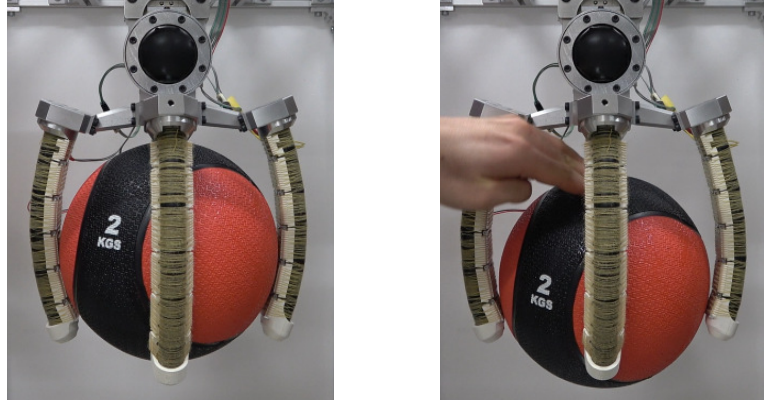


Figure 12. Experimental scenes where a disturbance was added manually in the vertical direction while the gripper was holding the 2 kg medicine ball.

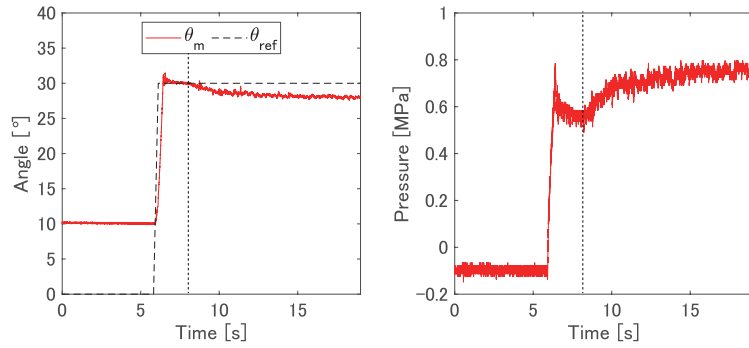


Figure 13. Values of the finger angle and pressure in the experiment shown in Fig. 12.

demonstrate a robustness to vertical-direction disturbance in this study.

Fig. 11 shows a block diagram of the 2-DOF control that we implemented in [21]. The reference value of the pressure is given by

$$P_{ref} = f(\theta_{ref}) + K_P \theta_e + K_I \int \theta_e dt \quad (30)$$

$$\theta_e := \theta_{ref} - \frac{1}{n} \sum_{j=1}^n \theta_j \quad (31)$$

where $f(\theta_{ref})$ is the feedforward term obtained by (26), and K_P and K_I are PI gains. As defined in (31), we fed back the error between the reference angle θ_{ref} and the average angle of all fingers.

Fig. 12 shows experimental scenes where a disturbance was added manually in the vertical direction while the gripper was holding the 2 kg medicine ball. Fig. 13 shows the values of the finger angle and the pressure in the experiment, in which the vertical dashed line indicates the moment when the downward disturbance was added. It is observed that higher pressure was generated by the pump to keep holding the ball.

	Self weight [g]	Payload-to-weight ratio	Type
(A) [33]	0.4	16000	Kirigami
(B) [34]	1.5	1086	Electro-adhesion
(C) [35]	97	123	Pneumatics (negative pressure)
(D) [16]	277	18	Pneumatics (positive pressure)
Ours	1130 ¹	17.7	Hydraulics (positive pressure)

Table 4. Comparison of payload-to-weight ratio with other soft robot grippers.

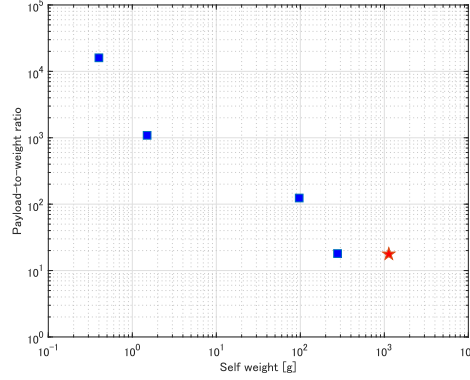


Figure 14. Payload-to-weight ratio versus the mass of soft grippers compared in Table 4

5. Discussions

5.1. Payload-to-weight Ratio

The weight of the developed soft gripper excluded the actuation unit is 1.13 kg. As an actuation source is usually built outside in most soft grippers, we calculate the payload-to-weight ratio as 17.7 ($\simeq 20/1.13$) using the weight excluding the actuation unit. We compare this value with other soft grippers that have high payload-to-weight ratio. Table 4 shows the comparison of the payload-to-weight ratio, including the actuation type of each soft gripper, and Fig.14 shows a plot of the payload-to-weight ratio versus the weight of soft grippers. Note that the vertical and horizontal axes of Fig.14 are log scales. Soft grippers using Kirigami structure [33] or electro-adhesion [34] achieved high payload-to-weight-ratio (16000 in [33] and 1086 in [34]) with light self-weight less than a few grams. However, the payload-to-weight ratio tends to decrease as the self weight increases. This implies that the payload-to-weight ratio does not always scale to larger weight. The payload-to-weight ratio of our soft gripper is as large as that of Yap et al. [16], but slightly larger than a line approximated by least-square of the other soft grippers [16,33–35]. Rather, we consider that an advantage of the developed gripper compared to these studies is the capacity of a large size object with 20 – 30 cm diameter.

5.2. Calculation of Graspable Area

Furthermore, the obtained model can be used to visualize the conditions under which the gripper can grasp an object. The conditions for grasping an object were represented by (29). Fig. 15 shows the graspable area of an object when the gripper wraps an object. The vertical axis represents the driving pressure, the horizontal axis represents the bending angle, and the color difference indicates the magnitude of the grasping

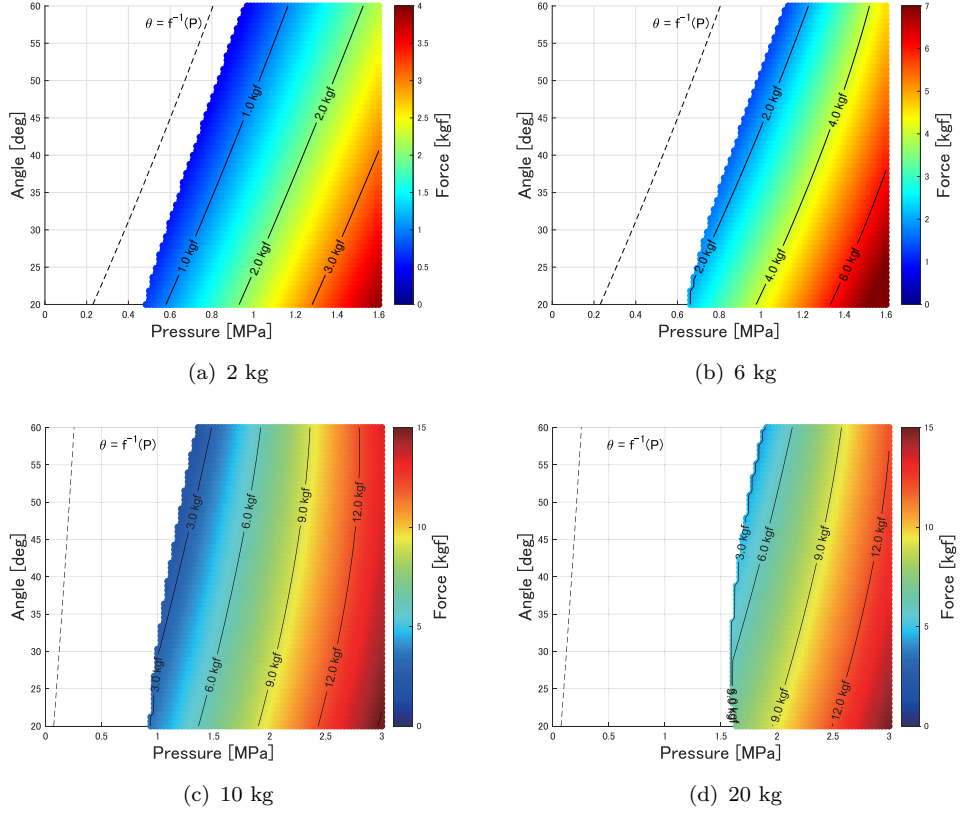


Figure 15. Relationship between the pressure and finger angle for different conditions of the object weight. Object are graspable in the colored area. The difference of color indicates the grasping force. The dotted line indicates the case without grasping an object, represented by (26).

force F_v . This relationship allows for calculating the pressure P required to grasp an object and the grasping force F_v when the approximate weight and size of the object are known by determining θ .

6. Conclusion

In this study, we developed a hydraulically-driven soft gripper and presented the design methodology for achieving the 20 kg payload. The key results are summarized as follows:

- (1) We selected appropriate material based on the result of the FEM analysis. When applying 4.0 MPa pressure, the maximum stress was 235.4 MPa at the fingertip cap and 170.3 MPa at the hinge joint in the fingertip. Since the fracture strength of PLA is 55 MPa, we selected A5052 for these parts due to its higher strength.
- (2) We estimated the maximum payload based on the previously developed model and the friction condition, and confirmed the maximum payload would be more than 20 kg. In the original estimation, we assumed the coefficients used in the model had the same value. However, the FEM analysis showed that the joint angle were different when the gripper grasped an object. Therefore, we determined the coefficient values from the FEM result, which was validated with the pre-

liminary experiment with the 6 kg object, and re-calculated the payload, which showed that the maximum payload was 20 kg when the total finger angle was 70°.

(3) The maximum payload was experimentally validated. We also experimentally demonstrated the adaptability of the developed soft gripper to various objects with different shape and size. Moreover, the closed-loop control of the finger angle demonstrated the robustness to vertical disturbances. These results imply that the developed soft gripper achieved the 20 kg payload without loosing the flexibility, adaptability and robustness.

Acknowledgement

This research was supported by the National Agriculture, Forestry and Fisheries Research Organization's International Competitiveness Enhancement Technology Development Project "Development of Agricultural Work Automation Technology Utilizing Robot Arms Suitable for Agricultural Products" (Research Leader: Takanori Fukao).

References

- [1] Shintake J, Cacucciolo V, Floreano D, et al. Soft robotic grippers. *Advanced materials*. 2018;30(29):1707035.
- [2] Rus D, Tolley MT. Design, fabrication and control of soft robots. *Nature*. 2015; 521(7553):467–475.
- [3] Fantoni G, Santochi M, Dini G, et al. Grasping devices and methods in automated production processes. *CIRP Annals*. 2014;63(2):679–701.
- [4] Zhang B, Xie Y, Zhou J, et al. State-of-the-art robotic grippers, grasping and control strategies, as well as their applications in agricultural robots: A review. *Computers and Electronics in Agriculture*. 2020;177:105694.
- [5] Wang Z, Hirai S, Kawamura S. Challenges and opportunities in robotic food handling: A review. *Frontiers in Robotics and AI*. 2022;8:789107.
- [6] Xavier MS, Tawk CD, Zolfagharian A, et al. Soft pneumatic actuators: A review of design, fabrication, modeling, sensing, control and applications. *IEEE Access*. 2022;10:59442–59485.
- [7] Gupta U, Qin L, Wang Y, et al. Soft robots based on dielectric elastomer actuators: A review. *Smart Materials and Structures*. 2019;28(10):103002.
- [8] Park SW, Kim SJ, Park SH, et al. Recent progress in development and applications of ionic polymer–metal composite. *Micromachines*. 2022;13(8):1290.
- [9] Xia Y, He Y, Zhang F, et al. A review of shape memory polymers and composites: mechanisms, materials, and applications. *Advanced materials*. 2021;33(6):2000713.
- [10] Pettersson A, Davis S, Gray JO, et al. Design of a magnetorheological robot gripper for handling of delicate food products with varying shapes. *Journal of Food Engineering*. 2010;98(3):332–338.
- [11] Guo J, Leng J, Rossiter J. Electroadhesion technologies for robotics: A comprehensive review. *IEEE Transactions on Robotics*. 2019;36(2):313–327.
- [12] Ruotolo W, Brouwer D, Cutkosky MR. From grasping to manipulation with gecko-inspired adhesives on a multifinger gripper. *Science Robotics*. 2021;6(61):eabi9773.
- [13] Amend J, Cheng N, Fakhouri S, et al. Soft robotics commercialization: Jamming grippers from research to product. *Soft robotics*. 2016;3(4):213–222.
- [14] Li S, Stampfli JJ, Xu HJ, et al. A vacuum-driven origami “magic-ball” soft gripper.

In: 2019 International Conference on Robotics and Automation (ICRA); IEEE; 2019. p. 7401–7408.

[15] Health and Safety Executive (UK). Manual handling operations regulations ; 1992. <https://www.hse.gov.uk/pubns/priced/123.pdf>.

[16] Yap HK, Ng HY, Yeow CH. High-force soft printable pneumatics for soft robotic applications. *Soft Robotics*. 2016;3(3):144–158.

[17] Hwang G, Park J, Cortes DSD, et al. Electroadhesion-based high-payload soft gripper with mechanically strengthened structure. *IEEE Transactions on Industrial Electronics*. 2021;69(1):642–651.

[18] Hagiwara K, Yamamoto K, Shibata Y, et al. On high stiffness of soft robots for compatibility of deformation and function. *Advanced Robotics*. 2022;36(19):995–1010.

[19] Azami O, Ishibashi K, Komagata M, et al. Development of hydraulically-driven soft hand for handling heavy vegetables and its experimental evaluation. In: 2023 IEEE International Conference on Robotics and Automation (ICRA); IEEE; 2023. p. 2577–2583.

[20] Ishibashi K, Komagata M, Ishikawa H, et al. Compact water pump and its application to self-contained soft robot hand for vegetable factory. *Advanced Robotics*. 2023;37(15):970–986.

[21] Ishibashi K, Ishikawa H, Azami O, et al. Modeling of hydraulic soft hand with rubber sheet reservoir and evaluation of its grasping flexibility and control (accepted). In: 2024 IEEE/RSJ International Conference on Intelligent Robots and Systems (IROS); IEEE; 2024.

[22] Suzumori K, Iikura S, Tanaka H. Flexible microactuator for miniature robots. In: [1991] Proceedings. IEEE Micro Electro Mechanical Systems; IEEE; 1991. p. 204–209.

[23] Deimel R, Brock O. A novel type of compliant and underactuated robotic hand for dexterous grasping. *The International Journal of Robotics Research*. 2016;35(1-3):161–185.

[24] Renda F, Boyer F, Dias J, et al. Discrete cosserat approach for multisegment soft manipulator dynamics. *IEEE Transactions on Robotics*. 2018;34(6):1518–1533.

[25] Renda F, Cacucciolo V, Dias J, et al. Discrete cosserat approach for soft robot dynamics: A new piece-wise constant strain model with torsion and shears. In: 2016 IEEE/RSJ International Conference on Intelligent Robots and Systems (IROS); IEEE; 2016. p. 5495–5502.

[26] Polygerinos P, Wang Z, Overvelde JT, et al. Modeling of soft fiber-reinforced bending actuators. *IEEE Transactions on Robotics*. 2015;31(3):778–789.

[27] Wang Z, Polygerinos P, Overvelde JT, et al. Interaction forces of soft fiber reinforced bending actuators. *IEEE/ASME Transactions on Mechatronics*. 2016;22(2):717–727.

[28] Mustaza SM, Elsayed Y, Lekakou C, et al. Dynamic modeling of fiber-reinforced soft manipulator: A visco-hyperelastic material-based continuum mechanics approach. *Soft Robotics*. 2019;6(3):305–317. PMID: 30917093; Available from: <https://doi.org/10.1089/soro.2018.0032>.

[29] Sedal A, Bruder D, Bishop-Moser J, et al. A continuum model for fiber-reinforced soft robot actuators. *Journal of Mechanisms and Robotics*. 2018;10(2):024501.

[30] Xavier MS, Fleming AJ, Yong YK. Finite element modeling of soft fluidic actuators: Overview and recent developments. *Advanced Intelligent Systems*. 2021;3(2):2000187.

[31] Barnard RW, Pearce K, Schovanec L. Inequalities for the perimeter of an ellipse. *Journal of mathematical analysis and applications*. 2001;260(2):295–306.

[32] Komagata M, Ko T, Nakamura Y. Design and development of compact ceramics reinforced pump with low internal leakage for electro-hydrostatic actuated robots. In: Advances in Mechanism and Machine Science: Proceedings of the 15th IFToMM World Congress on Mechanism and Machine Science 15; 2019. p. 2439–2448.

[33] Hong Y, Zhao Y, Berman J, et al. Angle-programmed tendril-like trajectories enable a multifunctional gripper with ultradelicacy, ultrastrength, and ultraprecision. *Nature Communications*. 2023;12:14.

[34] Cacucciolo V, Shintake J, Shea H. Delicate yet strong: Characterizing the electro-adhesion lifting force with a soft gripper. In: Proceedings of 2nd IEEE International Conference on

Soft Robotics (RoboSoft); 2019. p. 108–113.

[35] Li S, Stampfli JJ, Xu HJ, et al. A vacuum-driven origami “magic-ball” soft gripper. In: Proceedings of 2019 International Conference on Robotics and Automation (ICRA). IEEE; 2019. p. 7401–7408.